0026-895X/09/7505-1084–1095$20.00
MOLECULAR PHARMACOLOGY
Copyright © 2009 The American Society for Pharmacology and Experimental Therapeutics
Mol Pharmacol 75:1084–1095, 2009

Vol. 75, No. 5
54353/3463232
Printed in U.S.A.

Time-Resolved Photolabeling of the Nicotinic Acetylcholine Receptor by [^{3}H]Azietomidate, an Open-State Inhibitor

David C. Chiara, Filbert H. Hong, Enrique Arevalo, S. Shaukat Husain, Keith W. Miller, Stuart A. Forman, and Jonathan B. Cohen

Department of Neurobiology, Harvard Medical School, Boston, Massachusetts (D.C.C., F.H.H, J.B.C.); Department of Anesthesia and Critical Care, Massachusetts General Hospital, Boston, Massachusetts (E.A., S.S.H., K.W.M., S.A.F.); and Department of Biological Chemistry and Molecular Pharmacology, Harvard Medical School, Boston, Massachusetts (K.W.M.)

Received December 19, 2008; accepted February 13, 2009

ABSTRACT

Azietomidate is a photoreactive analog of the general anesthetic etomidate that acts as a nicotinic acetylcholine receptor (nAChR) noncompetitive antagonist. We used rapid perfusion electrophysiological techniques to characterize the state dependence and kinetics of azietomidate inhibition of *Torpedo californica* nAChRs and time-resolved photolabeling to identify the nAChR binding sites occupied after exposure to [^{3}H]azietomidate and agonist for 50 ms (open state) or at equilibrium (desensitized state). Azietomidate acted primarily as an open channel inhibitor characterized by a bimolecular association rate constant of $k_+ = 5 \times 10^5$ M^{-1} s^{-1} and a dissociation rate constant of <3 s^{-1}. Azietomidate at 10 μM, when perfused with acetylcholine (ACh), inhibited the ACh response by ~50% after 50 ms; when preincubated for 10 s, it decreased the peak initial response by ~15%. Comparison of the kinetics of recovery of ACh responses after exposure to ACh and azietomidate or to ACh alone indicated that at subsecond times, azietomidate inhibited nAChRs without enhancing the kinetics of agonist-induced desensitization. In nAChRs frozen after 50-ms exposure to agonist and [^{3}H]azietomidate, amino acids were photolabeled in the ion channel [position M2–20 (αGlu-262, βAsp-268, δGln-276)], in δM1 (δCys-236), and in αMA/αM4 (αGlu-390, αCys-412) that were also photolabeled in nAChRs in the equilibrium desensitized state at approximately half the efficiency. These results identify azietomidate binding sites at the extracellular end of the ion channel, in the δ subunit helix bundle, and in the nAChR cytoplasmic domain that seem similar in structure and accessibility in the open and desensitized states of the nAChR.

General anesthetics of diverse structures, including volatile and intravenous anesthetics and alcohols, modulate the function of members of the "Cys-loop" superfamily of neurotransmitter-gated ion channels either by potentiating agonist responses at inhibitory $GABA_A$ receptors and glycine receptors or by inhibiting responses of the excitatory serotonin 5-HT_3 and nicotinic acetylcholine receptors (nAChRs) (Yamakura et al., 2001; Arias et al., 2003; Hemmings et al., 2005). Each Cys-loop receptor is a pentamer of homologous or identical subunits that associate at a central axis that is the ion channel. Structural models can be derived from the structure of the muscle-type nAChR based upon cryoelectron microscope images of the *Torpedo marmorata* nAChR (Unwin, 2005), which provides a definition of the tertiary structure of the nAChR but lacks the resolution necessary to reliably define the positions of individual amino acids. The N-terminal half of each subunit contributes to the extracellular domain, containing the neurotransmitter binding sites that are located at subunit interfaces (α-γ and α-δ in the $\alpha_2\beta\gamma\delta$ *Torpedo californica* nAChR) 30 Å above the level of the membrane. Each nAChR subunit's transmembrane domain is made up of a loose bundle of four α helices (M1–M4), with amino acids from each M2 helix contributing to the lumen of the ion channel and M4 located most peripherally and in greatest contact with lipid. The structure of nAChR transmembrane domain suggests the existence of pockets within each subunit helix bundle and at subunit interfaces that are

This research was supported in part by the National Institutes of Health National Institute of General Medical Sciences [Grant GM58448] and by an award to Harvard Medical School from the Howard Hughes Biomedical Research Support Program for Medical Schools.
D.C.C. and F.H.H. contributed equally to this work.
Article, publication date, and citation information can be found at http://molpharm.aspetjournals.org.
doi:10.1124/mol.108.054353.

ABBREVIATIONS: 5-HT, 5-hydroxytryptamine; nAChR, nicotinic acetylcholine receptor; $GABA_AR$, GABA type A receptor; ACh, acetylcholine; EndoLys-C, *Lysobacter enzymogenes* endoproteinase Lys-C; V8 protease, *Staphylococcus aureus* endopeptidase Glu-C; Carb, carbamylcholine; PAGE, polyacrylamide gel electrophoresis; HPLC, high-pressure liquid chromatography; PTH, phenylthiohydantoin; QX-222, 2-((2,6-dimethylphenyl)amino)-*N*,*N*,*N*-trimethyl-2-oxoethanaminium; PAGE, polyacrylamide gel electrophoresis; TID, 3-(trifluoromethyl)-3-(*m*-iodophenyl)diazirine.

potential binding sites for general anesthetics and other allosteric modulators.

In the absence of agonist, the nAChR exists predominantly in a resting, closed channel conformation with low affinity for agonist that is in equilibrium with a nonconducting desensitized state with highest affinity for agonist. Agonist binding induces conformational transitions, within a fraction of a millisecond, to an open channel state (Maconochie and Steinbach, 1998), and desensitization occurs in two kinetically distinct phases over times from 0.1 to 100 s (Hess et al., 1983).

Mutational analyses identified positions within the M2 helices that can enhance or reduce the potency of aliphatic alcohols as open-state inhibitors (Zhou et al., 2000; Wenningmann et al., 2001; Borghese et al., 2002). Because these mutations often affect ACh gating in the absence of anesthetics, and they include substitutions at positions oriented toward the lumen of the ion channel and toward the interior of each subunit helix bundle or the interfaces with another subunit, it is difficult to determine whether the positions contribute directly to anesthetic binding or are involved in allosteric modulation of gating.

Photoaffinity labeling provides a method to directly identify amino acids contributing to a drug binding site in a protein without any prior assumptions about the location of the site (Kotzyba-Hibert et al., 1995; Vodovozova, 2007). State-dependent drug binding sites have been mapped by photolabeling *T. californica* nAChRs in the absence of agonist (resting state), equilibrated with agonist (desensitized state), and by the use of rapid-mixing and freeze-quench techniques (Arevalo et al., 2005), in the conformations transiently stabilized by agonist (for review, see Mourot et al., 2006).

R(+)-Etomidate, one of the most potent general anesthetics used clinically, acts at micromolar concentrations as an anesthetic and as a potentiator of the responses to submaximal concentrations of GABA, whereas at concentrations above 10 μM, it inhibits nAChRs. Azietomidate is a photoreactive etomidate analog that is equipotent with etomidate as a general anesthetic and as a positive allosteric modulator of $GABA_A$Rs (Husain et al., 2003; Liao et al., 2005). Photolabeling studies with [^{3}H]azietomidate identified a binding site in the $GABA_A$R transmembrane domain at the interface between the β and α subunits (Li et al., 2006). In the *T. californica* nAChR, azietomidate is equipotent with etomidate as a noncompetitive antagonist, binding with 10-fold higher affinity to the nAChR in the desensitized state than the resting state and photolabeling amino acids near the extracellular end of the ion channel domain only in the desensitized state (position M2–M20: αGlu-262 and δGln-276) (Ziebell et al., 2004). However, it is not known where (or whether) it interacts with nAChRs in the open channel state.

To provide a further definition of the diversity of binding sites and state dependence of binding of a single general anesthetic in a "Cys-loop" receptor, we use rapid perfusion electrophysiological techniques to characterize azietomidate's state dependence and kinetics of inhibition, and we use time-resolved photolabeling to identify the nAChR binding sites occupied after exposure to [^{3}H]azietomidate and agonist for 50 ms (open state) compared with the desensitized state.

Materials and Methods

Materials. nAChR-rich membranes were isolated from the electric organs of *T. californica* rays (Aquatic Research Consultants, San Pedro, CA) as described previously (Middleton and Cohen, 1991). The membranes, which contained 1 to 2 nmol of [^{3}H]acetylcholine (ACh) binding sites/mg of protein, were stored at −80°C in 38% sucrose.0.02% NaN_3. Azietomidate and [^{3}H]azietomidate (16 Ci/mmol; stored at a concentration of 14 μM in methanol at −80°C) were synthesized as described previously (Husain et al., 2003). Endoproteinase Lys-C (EndoLys-C) was from Roche Applied Sciences (Indianapolis, IN), *N*-tosyl-L-phenylalanine chloromethyl ketone-treated trypsin was from Worthington Biochemical (Lakewood, NJ), and *Staphylococcus aureus* endopeptidase Glu-C (V8 protease) was from MP Biomedicals (Solon, OH).

Animal Use. Female *Xenopus laevis* frogs (Xenopus One, Dexter, MI) were housed in a veterinarian-supervised environment in accordance with local and federal guidelines and with the approval of the institutional research animal care committee. Oocytes were harvested via minilaparotomy from frogs anesthetized with 0.1% tricaine methanesulfonate.

Oocyte Expression of *T. californica* nAChRs. In vitro transcription of *T. californica* nAChR subunit-specific cRNAs and the protocols for the isolation and injection of *X. laevis* oocytes were carried out as described previously (Sullivan and Cohen, 2000). Isolated follicle-free oocytes were injected with 0.5 to 1 ng of subunit RNAs in a molar ratio of 2α/β/γ/δ and incubated at 18°C for 48 to 72 h before measurement of ACh responses. Under our experimental conditions, when responses for intact oocytes were measured by two-electrode voltage clamp, the maximal currents elicited by ACh were typically 1 to 2 μA. Oocytes were placed in 1 M *N*-methyl-D-glucamine for 5 to 20 min and then stripped manually of their vitelline membranes before isolation of detached patches.

Patch-Clamp Electrophysiology. Macroscopic currents were recorded from excised outside-out patches at room temperature (21–23°C). Fire-polished micropipettes for creating patches were pulled (P-97 Flaming/Brown Micropipette Puller; Sutter Instrument Co., Novato, CA) to a resistance of 1 to 3 MΩ. Pipets were filled with K-100 buffer (97 mM KCl, 0.2 mM EGTA, 5 mM K-HEPES, and 1 mM $MgCl_2$, pH 7.5), which was also used for external solutions. Oocyte patches were voltage-clamped at −50 mV, and currents through the patch clamp amplifier (Axopatch 200A; Molecular Devices, Sunnyvale, CA) were filtered (8-pole Bessel, 1–2 kHz) and digitized at 2 to 5 kHz by use of a Digidata 1200 interface and pClamp 8.0 (both from Molecular Devices).

Four-Channel Pipette Protocols. Rapid application of solutions to detached patches was achieved using a dual-axis, piezo-driven, four-barrel capillary tube (2 × 2) that allows switching between four flowing solutions, with an exchange time between adjacent solutions of <0.5 ms (Forman, 1999). Channel A of the quad tube was fed from a 100-ml syringe containing K-100 buffer; channel B contained 300 μM ACh, fed by a 15-ml syringe. Channels C and D were fed by manifolds of six 15-ml syringes, each of which had individual valves to allow simple changes in stream contents, and these channels were used to perfuse the patch with variable concentrations of ACh, azietomidate, or combinations of ACh and azietomidate. The stability of patch responses was monitored before each experiment and after each change of agonist or antagonist concentration by a control protocol: 50 ms in buffer (channel A), followed by 800-ms exposure to 300 μM ACh (channel B), then 150 ms in buffer, repeated four times with a 10- to 15-s delay between each iteration. To determine the ACh dose-response and the concentration dependence of azietomidate inhibition, the patch was first perfused with buffer (channel A), then switched to channel C containing either a test concentration of ACh or 300 μM ACh and a test concentration of azietomidate, and then returned to channel A. For each azietomidate or ACh concentration series, measurements were performed in order of increasing concentration. The amount of time spent in each step

varied between experiments and is noted in the text and figure legends. For azietomidate preincubation experiments, a patch was moved from buffer (channel A) to channel C containing azietomidate (10 μM) for a variable amount of time and then to channel D containing 300 μM ACh and azietomidate. Recordings were averages of four to six sweeps, with 20 to 30 s between trials and ACh control measurements taken after each condition was tested.

Three protocols were used to determine the effects of azietomidate on the kinetics of desensitization of the nAChR response. 1) The onset and recovery from agonist-induced desensitization was determined by switching a patch from buffer to 300 μM ACh for 2 s, at which time the patch was returned to buffer, with the recovery of the response monitored at intervals by returning the patch briefly (50 ms) to 300 μM ACh. 2) To determine whether azietomidate enhanced the kinetics of desensitization, the patch was moved from buffer to 300 μM ACh and 10 μM azietomidate (channel D) for 2 s and then the patch was returned to buffer, with the recovery of the response monitored at intervals by return of the patch to ACh and azietomidate (channel D) for 50 ms. 3) To test for the recovery from desensitization in the presence of azietomidate, after exposure to ACh + azietomidate (channel D) for 2 s, the patch was moved to 10 μM azietomidate alone (channel C) and then returned at intervals to ACh + azietomidate for 50 ms.

Data Analysis. Agonist dose response curves were fit to the equation $I = I_{max}/[1 + (K_{app}/x)^{n_H}]$, where I and I_{max} are the current at agonist concentration x and the maximum current, respectively, K_{app} is the agonist concentration for half-maximal response, and n_H is the Hill coefficient. The concentration dependence of drug inhibition of ACh-induced currents was fit to the equation $I = I_0/[1 + (x/IC_{50})]$, where I is the current in the presence of inhibitor concentration x, I_0 is the current in the absence of inhibitor, and IC_{50} is the inhibitor concentration producing 50% inhibition. SigmaPlot (Systat Software, Inc., San Jose, CA) was used for the nonlinear least-squares fit of the data, and the standard errors of the parameter fits are indicated. The observed decline of the response from the peak initial response either in the presence of ACh alone (desensitization) or of ACh and azietomidate was fit to $I_t = I_\infty + (I_{pk} - I_\infty)\exp^{-kt}$, where t is time, I_∞ is the residual response at long times, I_{pk} is the peak initial current, and k is the rate constant. The kinetics of recovery of the response after exposure to ACh with or without azietomidate for seconds were fit to the equation $I = I_{rec} - a_s\exp^{-bt}$, where I_{rec} is the current after full recovery, a_s is the amplitude of the observed slow recovery on the time scale of seconds, and b is the rate constant (see Fig. 3A). The amplitude of the rapid phase of recovery, a_f, is equal to $I_{rec} - (a_s + I_f)$.

Photolabeling nAChR-Rich Membranes. For photolabeling studies, [^{3}H]azietomidate was isotopically diluted to 1.6 Ci/mmol with an appropriate volume of nonradioactive azietomidate at 1 mg/ml in methanol, which was removed via evaporation immediately before the addition of *T. californica* physiological saline (250 mM NaCl, 5 mM KCl, 3 mM $CaCl_2$, 2 mM $MgCl_2$, and 5 mM $NaPO_4$, pH 7.0) with or without *T. californica* nAChR-rich membranes resuspended at 4 mg of protein/ml. The freeze-clamp apparatus and method were described previously (Addona et al., 1999; Arevalo et al., 2005). In brief, two syringes driven by a pneumatic ram were upstream of two sample loops loaded with the solutions to be mixed. When the pneumatic ram was activated, the solutions were forced through a mixer (<1 ms) and an aging tube onto a rotating stainless steel disk precooled to liquid nitrogen temperatures. In general, one sample loop contained 0.5 ml of nAChR membranes, sometimes premixed with [^{3}H]azietomidate and/or agonist [carbamylcholine (Carb)], and the other contained 0.5 ml of *T. californica* physiological saline, Carb, and/or [^{3}H]azietomidate. After mixing, the final concentrations were 2 mg of membrane protein/ml, 10 μM [^{3}H]azietomidate, and 10 mM Carb. Stainless steel tubing was used throughout. The membranes on the freezing plate, which was rotating slowly in contact with liquid nitrogen, were then irradiated (Blak-Ray UV lamp model UVL-56; UVP, Inc., Walnut Grove, CA) for 30 min at 365 nm at a distance of ~3 cm. After irradiation, the frozen membranes were collected with precooled forceps and stored at −80°C. To obtain sufficient material for identification of labeled amino acids, material was pooled from six samples photolabeled in the frozen state in each condition, and 12 samples could be photolabeled in a day. Carb, an ACh analog resistant to hydrolysis by acetylcholinesterase, was used as the agonist for photolabeling studies because of the high concentrations of the esterase in the nAChR-rich membranes. For native *T. californica* nAChR in sealed vesicles, Carb produces a maximal flux response close to that of ACh with a concentration dependence characterized by a K_{app} of 1 mM (i.e., 20-fold higher than that of ACh) (Forman et al., 1987).

Gel Electrophoresis and Proteolytic Digestions. Frozen samples (~1 ml and 1–2 mg protein) were thawed individually in 0.2 ml of 10% SDS. Aliquots (~100 μl) were removed for protein assay (MicroBCA; Pierce, Rockford, IL) and analysis by analytical SDS-PAGE, and the six samples for each condition (~ 6 ml) were then pooled and combined with 4× sample buffer (final concentration, 8% sucrose, 2% SDS, 0.06 M Tris, 2.5% β-mercaptoethanol, 0.4% glycerol, and 0.0025% bromphenol blue, pH 6.8) for isolation of nAChR subunits by SDS-PAGE on 1.5-mm thick acrylamide (8%) slab gels. Because of the large sample volumes, the loading wells were ~6 cm deep, and the stacking and resolving gels were ~3 and 15 cm long. After staining with Coomassie blue, the gel bands containing the β, γ, and δ subunits were excised and eluted passively for 3 days into 12 ml of elution buffer (100 mM NH_4HCO_3, 2.5 mM dithiothreitol, and 0.1% SDS, pH 8.4). The bands containing the α subunit were excised and layered onto a second, 15% acrylamide gel for limited digestion "in gel" with *S. aureus* V8 protease (White and Cohen, 1988). After electrophoresis, that gel was stained with GelCode Blue (Pierce), and the proteolytic fragments of 20 (αV8–20), 18 (αV8–18), and 10 kDa (αV8–10) were excised and eluted. The eluates were filtered and concentrated to <400 μl by centrifugal filtration. nAChR subunits or subunit fragments were acetone precipitated in 75% acetone (12 h at −20°C), and the pellets were resuspended in 100 to 200 μl of digestion buffer (15 mM Tris, 0.5 mM EDTA, 0.1% SDS, pH 8.1). Protease digests of αV8–20 and αV8–10 were fractionated directly by reversed-phase HPLC, whereas digests of the β and δ subunits were fractionated on 1.5-mm Tricine SDS-PAGE gels (Schägger and von Jagow, 1987), which were then cut into 5-mm bands and the material eluted to identify the bands containing ^{3}H, which were then concentrated and fractionated by reversed-phase HPLC.

The αV8–20 fragment and δ subunit were digested with EndoLys-C (0.75 U in 10 μl of distilled water per sample) for 2 weeks at 25°C. For digestion with trypsin, the β subunit and the αV8–10 fragment in resuspension buffer were diluted 5-fold with 100 mM NH_4HCO_3, 0.5% Genapol C-100 (CalBiochem, San Diego, CA), pH 8.1, and trypsin (100 μg, in 20 mM $CaCl_2$ at 1/10 the volume of the material to be digested) was then added for digestion at 25°C overnight (β subunit) or for 3 days (αV8–10).

Reversed-Phase HPLC. Samples were fractionated using a Brownlee Aquapore BU-300 7 μm 100 × 2.1-mm column with a NEWGUARD RP-2 7 μm guard column on an Agilent 1100 binary system (Agilent Technologies, Santa Clara, CA) with an in-line solvent degasser, a column compartment (temperature held at 40°C), and attached UV absorbance (215 nm) and fluorescence detectors. The aqueous phase was 0.08% trifluoroacetic acid, the organic phase was 60% acetonitrile, 40% isopropanol, and 0.05% trifluoroacetic acid, the flow rate was 200 μl/min, and the gradient used is included on HPLC trace figures as a dashed line. Fraction volumes were 500 μl, of which 10% was assayed for ^{3}H.

Sequence Analysis. N-terminal sequencing was performed on a Procise 492 protein sequencer (Applied Biosystems, Foster City, CA), modified such that one sixth of the PTH-amino acid solution from each cycle was injected into the amino acid analyzer and the other 5/6 of the sample was sent to a fraction collector for ^{3}H-quantitation. Most HPLC fractions were drop-loaded onto glass fiber filters (Ap-

plied Biosystems) at 45°C, with BioBrene Plus (Applied Biosystems) added after loading to avoid heat-induced peptide bond cleavage at tryptophans (Chiara et al., 2003). Fractions containing αM4 or δM1, which are not sequenced efficiently on glass fiber filters, were loaded for sequencing onto ProSorb polyvinylidene difluoride filter cartridges (Applied Biosystems).

The amount of released PTH derivative in each cycle, which was determined by comparison with standards from the background-corrected peak height using the model 610A Data Analysis Program (Applied Biosystems), is shown in the figures along with the ^{3}H released in each cycle. To determine the amount of peptide in each sample, the background-subtracted number of pmol detected ($f(x)$) in cycle x was fit to the equation $f(x) = I_0 \times R^x$, and the equation was solved for I_0 (initial peptide amount) and R (average repetitive yield).

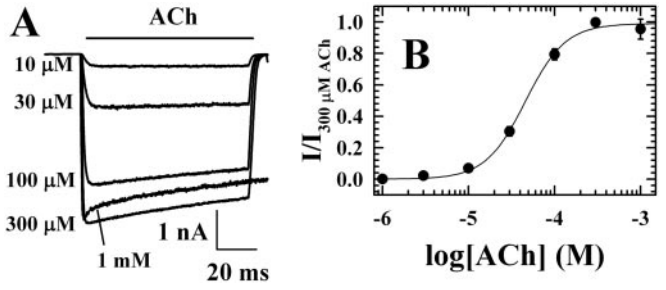

Fig. 1. Responses to ACh measured by rapid perfusion of *T. californica* nAChRs in detached patches. A, representative macroscopic current responses when an "outside-out" patch at a holding potential of −50 mV was exposed to varying concentrations of ACh for 100 ms. Each trace is the average of four sweeps, with 20 s between each sweep. B, the concentration dependence of the peak ACh responses, with data from two patches normalized to the response to 300 μM ACh and error bars indicating the range. The response was fit by $K_{app} = 43 \pm 4$ μM and $n_H = 1.9 \pm 0.2$.

Ser, Cys, Arg, His, and Trp residues were excluded from the fit because of known problems with their quantitation. Unless otherwise noted, the efficiency of labeling of an amino acid (cpm per picomole) was calculated as $(cpm_x - cpm_{x-1})/(5 \times I_0 R^x)$.

Molecular Modeling. The *T. marmorata* nAChR structure (Protein Data Bank 2BG9) was used to model the interactions of azietomidate with the receptor in the photolabeled regions using the Discovery Studio molecular modeling package (Accelrys, San Diego, CA). Docking studies were performed using CDocker by starting with a minimized model of azietomidate placed in existing pockets within the structure adjacent to labeled residues using a binding site sphere 15 to 18 Å in radius. The program then identified 100 possible solutions; for visualization, each binding pocket was represented by the Connolly surface, defined by a 1.8-Å diameter probe, of the ensemble of the 10 docking solutions with the most favorable binding energies (Fig. 8).

Results

nAChR Inhibition by Azietomidate. When ACh responses were measured by rapid perfusion of nAChRs in detached, "outside-out" patches held at −50 mV, the concentration dependence of the ACh response was characterized by a K_{app} of 40 μM and a Hill coefficient, n_H, of 2 (Fig. 1). Representative current traces are shown in Fig. 1A for *T. californica* nAChRs exposed to ACh concentrations from 10 μM to 1 mM. ACh at 300 μM produced a maximal response in several milliseconds, and the current response then decreased by ~20% in 100 ms. ACh at 1 mM produced a similar initial peak response, which was followed by a rapid decline of ~10%, presumably as a result of channel block, and then by a further decline at a rate similar to that seen at 300 μM ACh.

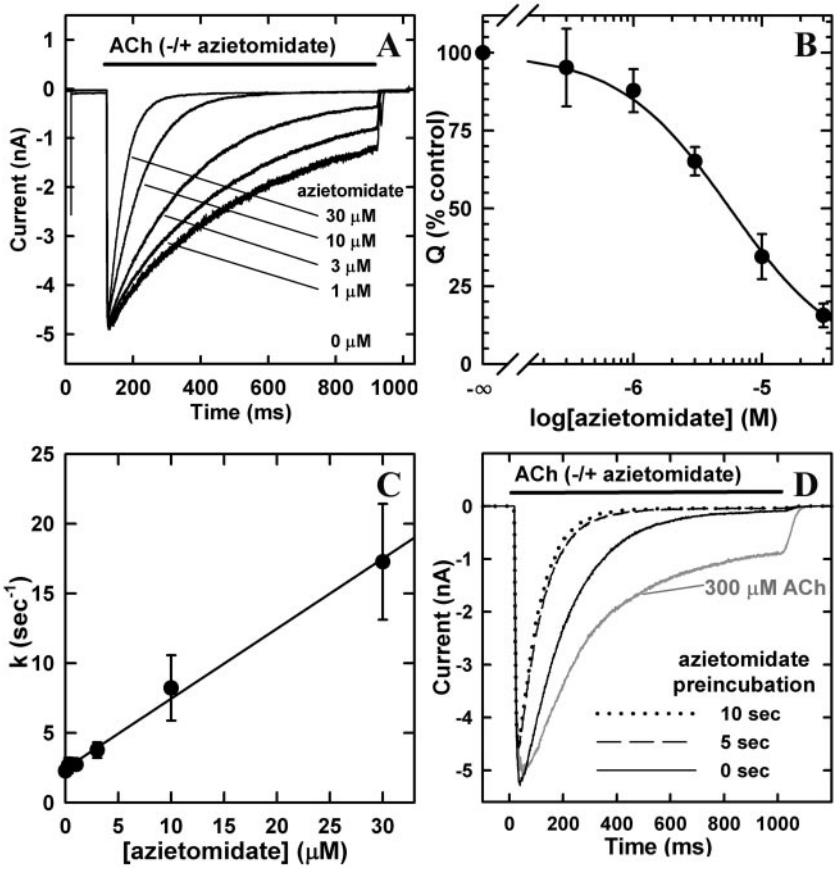

Fig. 2. Azietomidate inhibition of *T. californica* nAChRs. Azietomidate inhibition of ACh responses of *T. californica* nAChRs expressed in *X. laevis* oocytes was measured by rapid perfusion of outside-out patches detached from oocytes. A, representative macroscopic current traces from a single patch exposed for 800 ms to 300 μM ACh coapplied with increasing concentrations of azietomidate. For each concentration, the current traces are the average of four repetitions, with 10 s between each sweep. Each trace was normalized to the peak current response for 300 μM ACh applied before each exposure to azietomidate. After exposure to 30 μM azietomidate and 10 s recovery, the peak ACh current was >90% of the previous control, and τ_{des} was decreased by <20% compared with the value before exposure to any azietomidate. B, the concentration dependence of azietomidate inhibition. Responses were measured by the net charge transfer during 800-ms exposure to ACh and azietomidate, normalized for each patch to the value for ACh alone. Data are the mean ± S.E.M. from four patches, and the calculated IC_{50} was 5.6 ± 0.2 μM. C, dependence of the kinetics of inhibition on azietomidate concentration. For each concentration of azietomidate, the observed decline of the response at time t from the peak was fit to a single exponential: $I_t = I_\infty + (I_{pk} - I_\infty)\exp^{-kt}$. I_∞ is the residual response at long times, I_{pk} is the peak initial current, and k is the rate constant. Inhibition rates (mean ± S.E.M., three patches) are plotted against azietomidate concentration. Linear least-squares regression gives a slope of $5.0 \pm 0.2 \times 10^5$ M^{-1} s^{-1}. D, effect of azietomidate preincubation on the inhibition of *T. californica* nAChRs in excised patches. The responses of nAChRs exposed to 300 μM ACh and 10 μM azietomidate are shown for a single patch. Before each ACh application, the patch was perfused with 10 μM azietomidate for 0, 5, or 10 s. The calculated net charge transfer during the 1-s response was 2.0 nC for the control in the absence of azietomidate, and 1.1, 0.54, and 0.48 nC after 0, 5, and 10 s of preincubation, respectively.

To test the effects of azietomidate, nAChRs were exposed simultaneously for 800 ms to 300 μM ACh and azietomidate at concentrations varying from 1 to 30 μM (Fig. 2). For 300 μM ACh alone, the decline from the peak current response (agonist-induced desensitization) was well fit by a single exponential characterized by τ of ~450 ± 75 ms (n = 5), with the current responses decreasing by ~75% after 800 ms. Exposure to increasing concentrations of azietomidate reduced the peak initial responses by less than 5%, but there was a concentration-dependent increase in the rate and extent of the decline of the response from the peak. In the presence of 10 μM azietomidate, ACh responses were inhibited by ~50% after ~60 ms and by ~98% by 800 ms. Etomidate over a similar concentration range had the same effect on ACh responses (data not shown). When the concentration dependence of inhibition was quantified by measuring the net charge transfer during the 800-ms exposure period, the IC_{50} for azietomidate inhibition was 6 ± 2 μM (n = 4) (Fig. 2B), whereas for etomidate, the IC_{50} was 7 ± 4 (n = 2).

Azietomidate at increasing concentrations enhanced the rate and extent of the decline of the ACh response. At all concentrations, that decline was well fit by a single exponential, and the rate increased linearly with azietomidate concentration (Fig. 2C). Although the kinetics of decline of the response in the presence of ACh alone reflects the kinetics of agonist-induced desensitization, the observed concentration-dependent inhibition by azietomidate could reflect either enhanced kinetics of desensitization or the kinetics of binding of azietomidate. Assuming the latter case, the observed inhibition would be consistent with an apparent bimolecular association rate constant for azietomidate of 5.0 ± 0.2 × 10^5 M^{-1} s^{-1} (data from three patches). Additional experiments, described below, establish that the nAChRs inhibited by azietomidate are not in the desensitized state that is stabilized by agonist.

Preincubation with azietomidate had only subtle effects on the inhibition of the ACh response (Fig. 2D). Prior exposure to 10 μM azietomidate for either 5 or 10 s resulted in a decrease of the peak initial response by ~15% and a doubling in the rate of decline of the ACh response compared with simultaneous addition.

Recovery from Inhibition. To determine whether azietomidate stabilized the same nAChR-desensitized state as ACh, we measured the kinetics of recovery of ACh responses after exposure to 300 μM ACh alone for 2 s or to ACh and 10 μM azietomidate (Fig. 3). The general features of the ACh response expected for such a protocol are schematized in Fig. 3A, and experimental data are shown for patches exposed only to buffer during the recovery period (Fig. 3B) or exposed to 10 μM azietomidate throughout the recovery period (Fig. 3C), with the parameters characterizing the recovery kinetics in Table 1.

After exposure to either ACh or ACh and azietomidate, recovery occurred in two phases: a rapid phase (amplitude, a_f), complete within 100 ms, and a slow phase (amplitude, a_s), characterized by τ_s ~0.7 s). For the ACh controls, the response decreased by 70% during the 2-s application of ACh, whereas in the presence of ACh and azietomidate, the response decreased to baseline. For the ACh controls, 80 to 85% of the recovery occurred during the slow phase. After exposure to ACh and azietomidate, the observed recovery was similar whether or not azietomidate was present during the recovery phase. In both conditions, after 100-ms recovery, the ACh response was close to that seen after desensitization by ACh alone. Thus, the rapid phase of recovery was larger after

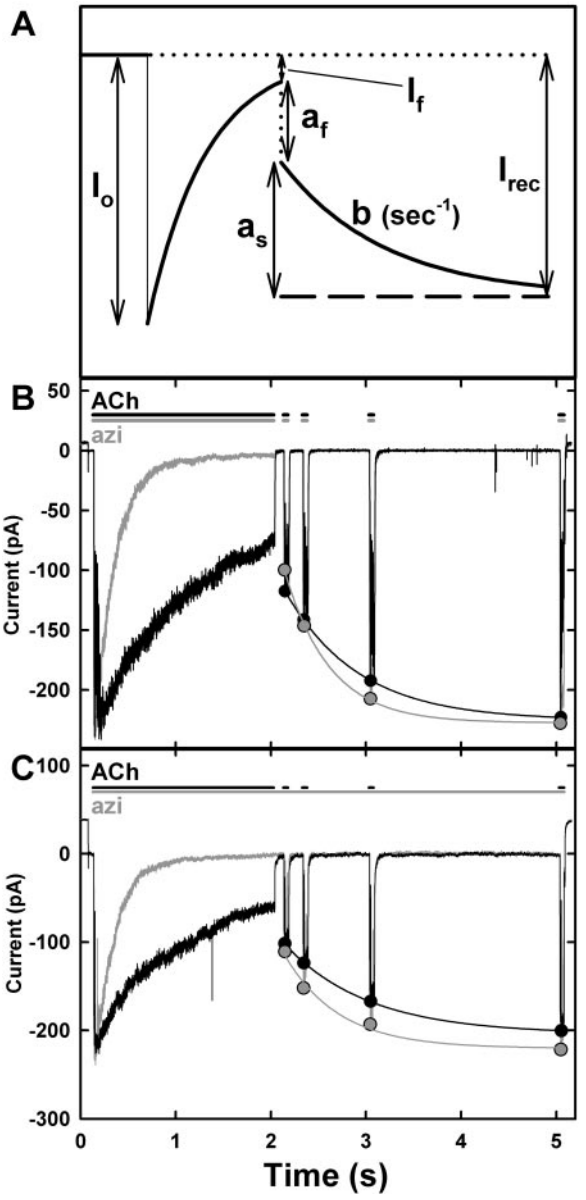

Fig. 3. Recovery of ACh responses after inhibition by azietomidate. A, a schematic defining the parameters characterizing the kinetics of recovery of ACh responses after exposure to ACh in the absence or presence of azietomidate. After exposure to a stream of ACh ± azietomidate, the patch was switched to a stream that contains buffer, with ACh sensitivity monitored by moving the patch for 50 ms into 300 μM ACh + azietomidate after 0.1, 0.3, 1.0, and 3.0 s of recovery. I_0 is the peak initial response to 300 μM ACh ± 10 μM azietomidate; I_f is the current after 1.95 s. The observed recovery was fit to a single exponential: $I = I_{rec} - a_s \exp^{-bt}$, where I_{rec} is the current after full recovery, a_s is the amplitude of the observed slow recovery on the time scale of seconds, and b is the rate constant The amplitude of the rapid phase of recovery, a_f, is equal to $I_{rec} - (a_s + I_f)$. B and C, experimental traces from two patches. The black traces are the ACh controls (1.95-s exposure to 300 μM ACh, followed by recovery in buffer with test pulses of 300 μM ACh), and the gray traces are the currents seen during exposure to ACh + 10 μM azietomidate, followed by recovery in buffer alone (B) or in a stream containing 10 μM azietomidate (C), with recovery tested by exposure to 300 μM ACh and 10 μM azietomidate. Traces shown in B and C are the average of four to six sweeps, each with 20 to 30 s between each sweep. The parameters characterizing the recovery kinetics are detailed in Table 1.

exposure to ACh and azietomidate than to ACh alone, whereas the slow phase occurred with an amplitude and kinetics similar to that seen for ACh alone. These results establish that when azietomidate inhibits the nAChR in the presence of ACh, it does not do so by stabilizing the ACh-induced desensitized state.

Comparison of nAChR Inhibition by Azietomidate and QX-222. To further characterize the state of the nAChR inhibited by azietomidate, two additional rapid perfusion protocols were used to compare nAChR inhibition by azietomidate with inhibition by QX-222, which acts as an open channel blocker characterized by rapid association and dissociation [$k_+ = 4 \times 10^7\ M^{-1}\ s^{-1}$, $k_- = 1 \times 10^3\ s^{-1}$ (Dilger and Vidal, 1994)]. In one protocol, nAChRs were exposed to ACh and QX-222 or azietomidate and then returned to buffer. After exposure to ACh and QX-222, the current was ~30% of control (ACh alone) after 30 ms, and a transient increase in current ("rebound" current) was seen after the patch was moved to buffer, which results from ion flow through open channels as QX-222 dissociates (Fig. 4A). For nAChRs exposed to 300 μM ACh and 10 μM azietomidate, the current was at ~50% of control (ACh alone) after 100 ms, and when the patch was then switched to buffer, the current decreased within milliseconds to baseline without evidence of any "rebound" current (Fig. 4C). Thus, azietomidate did not act as an open channel blocker characterized by rapid dissociation.

In a second protocol, responses were measured when the patch was shifted from ACh and QX-222 or azietomidate to ACh alone. After exposure to ACh and QX-222 for 30 ms, when the patch was returned to ACh, the current rapidly increased to the level seen for ACh alone (Fig. 4B), which indicates that QX-222 dissociates rapidly from nAChRs that had been inhibited without any increase in the fraction in the desensitized state. When the patch was moved to a stream of ACh after 30-ms exposure to ACh and azietomidate, the current neither increased to control levels as seen for QX-222 nor declined as in the continued presence of azietomidate. Rather, the current response declined at a rate similar to the control ACh response (Fig. 4D). This response suggests that the nAChRs that had bound azietomidate within 30 ms remained occupied and inhibited during the subsequent 200-ms exposure to ACh, whereas ACh binding to the nAChRs that had not bound azietomidate resulted in channel gating and then desensitization.

TABLE 1

Kinetics of recovery of ACh responses after inhibition by azietomidate

nAChRs in detached patches were exposed for 2 s to 300 μM ACh ± 10 μM azietomidate, and then returned to buffer, with ACh sensitivity monitored at intervals by moving the patch for 50 ms to a test solution of 300 μM ACh + azietomidate (Fig. 3). I_0 is the peak initial response to 300 μM ACh ± 10 μM azietomidate; I_f is the current after 1.95 s. The observed recovery was fit to a single exponential: $I = I_{rec} - a_s \exp^{-bt}$, where I_{rec} is the current after full recovery, a_s is the amplitude of the observed slow recovery on the time scale of seconds, and b is the rate constant. The amplitude of the rapid phase of recovery, a_f, is equal to $I_{rec} - (a_s + I_f)$. See Figure 3A for a definition of the parameters.

	I_0	I_f/I_0	I_{rec}	a_s	$\tau_s = b^{-1}$	a_f
	pA		*pA*	*pA*	*ms*	*pA*
Figure 3B						
ACh	2200.31		206 ± 1	115 ± 1	770 ± 20	21.4
ACh + azietomidate	2410.02		228 ± 2	161 ± 4	470 ± 30	61.6
Figure 3C						
ACh	2260.27		204 ± 1	116 ± 1	880 ± 40	27.9
ACh + azietomidate	2390.002		220 ± 10	129 ± 15	570 ± 190	90.5

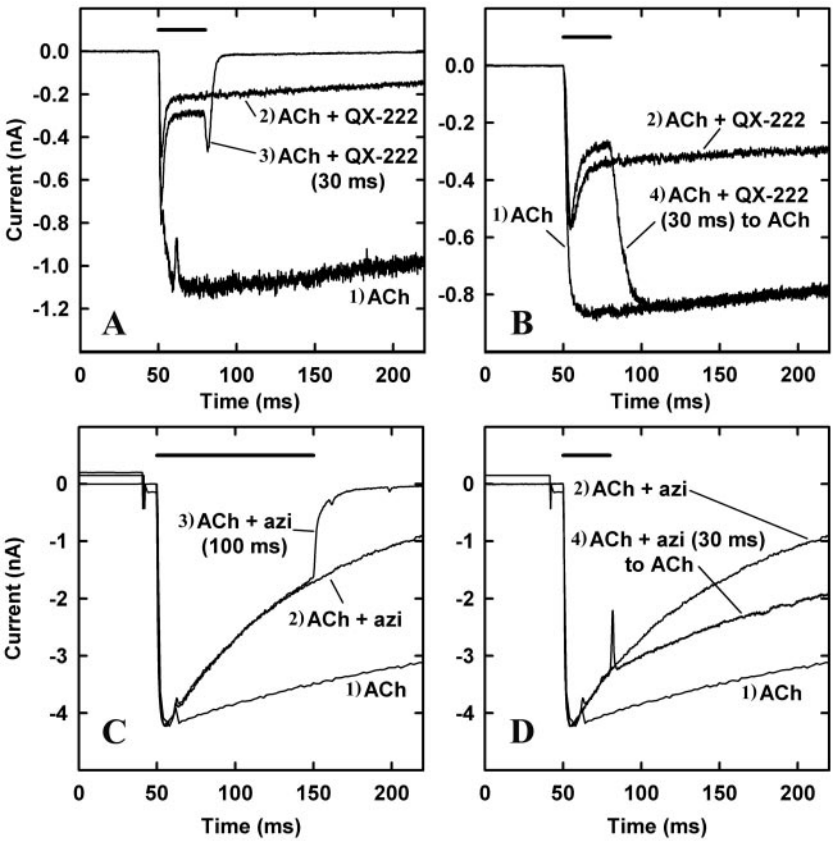

Fig. 4. Comparison of nAChR inhibition by the open channel blocker QX-222 (100 μM, A and B) and by azietomidate (10 μM, C and D). *T. californica* nAChRs were exposed simultaneously to 300 μM ACh and inhibitor according to four different protocols that are numbered on the traces: 1) 800 ms of ACh, before return to buffer; 2) 800 ms of ACh + inhibitor, before return to buffer; 3) 30 ms of ACh + QX-222 (A) or 100 ms of ACh + azietomidate (C), before return to buffer; or 4) 30 ms of ACh + QX-222 (B) or ACh + azietomidate (D), before return to ACh alone for 170 ms. In each panel, the bar above the current traces indicates the duration of exposure to ACh and QX-222 or azietomidate before switching the patch to a stream of buffer (A and C) or ACh (B and D). A and B are all from a single patch, as are those from C and D. Each trace is an average of four sweeps, with a 20- to 120-s buffer wash between each trial.

[^{3}H]Azietomidate Photolabeling of nAChRs Frozen after 50-ms Exposure to Agonist. For nAChRs exposed to an agonist concentration producing a maximal response, the electrophysiological analyses established that there was little desensitization within 50 ms and that simultaneous exposure to 10 μM azietomidate inhibited the response by ~50%, with no evidence that the inhibition was associated with stabilization of nAChRs in the slowly reversible desensitized state stabilized by agonist. Therefore, to characterize [^{3}H]azietomidate photolabeling when a maximal fraction of nAChRs are in the open state, nAChRs were frozen for photolabeling 50 ms after exposure to [^{3}H]azietomidate at a final concentration of 10 μM and with the agonist carbamylcholine (Carb) at a concentration (10 mM), which produces a maximal response for native *T. californica* nAChRs in sealed vesicles (Forman et al., 1987). This photolabeling condition will be referred to as "Open," although these nAChRs will be distributed in the multiple conformational states transiently stabilized by agonist [open, "preopen" (Lape et al., 2008), and fast-desensitized]. In parallel, nAChRs pre-equilibrated with 10 mM Carb were photolabeled when frozen after 50 ms exposure to 10 μM [^{3}H]azietomidate and 10 mM Carb (Des, agonist desensitized state). Table 2 summarizes for comparison purposes the efficiencies (cpm/mol) of [^{3}H]azietomidate photolabeling of nAChR amino acids in each of the photolabeling conditions.

Photolabeled amino acids in the α subunit transmembrane domain were identified by isolating labeled fragments from proteolytic digests of two large subunit fragments that are produced by digestion "in gel" with V8 protease (White and Cohen, 1988): a 10-kDa fragment (αV8–10, beginning at αAsn-339 and containing αM4) and a 20-kDa fragment (αV8–20, beginning at αSer-162/173 and containing M1-M3). When the trypsin digest of αV8–10 was fractionated by reversed-phase HPLC (Fig. 5A), ~80% of ^{3}H was recovered in or near the flow-through fractions, and ~20% was recovered in a broad hydrophobic peak (70–95% organic) that is known to contain the fragments spanning αM4. Sequence analysis of the pool of the hydrophobic peak (Fig. 5B) revealed the presence of a primary sequence beginning at αSer-388, extending through αLys-400 and αM4, and a secondary sequence beginning at αTyr-401. The major peak of ^{3}H release was in cycle 3, with a smaller peak of release in cycle 12. The ^{3}H release in cycle 3 resulted from labeling of αGlu-390 in the primary sequence (Open, 1.2 cpm/pmol; Des, 0.6 cpm/pmol), because labeling of αAla-403 in the secondary sequence would have also resulted in a peak of ^{3}H release in cycle 16 from the primary sequence, which was not seen. The ^{3}H release in cycle 12 probably resulted from labeling of αCys-412 in the secondary sequence (Open, 0.9 cpm/pmol; Des, 0.5 cpm/pmol), because there were also low peaks of ^{3}H release in cycle 25. Because [^{3}H]azietomidate photolabels αGlu-390, at least some of the ^{3}H in the HPLC flow-through fractions of Fig. 5A must result from the presence of labeled αGlu-390 in the hydrophilic peptides also generated when αV8–10 is cleaved at αGlu-400 to produce the fragment beginning at αTyr-401. However, additional studies are required to determine whether [^{3}H]azietomidate photolabels other amino acids between αAsn-339 and αGlu-387 that would also be contained within the hydrophilic fragments produced by trypsin cleavage of αV8–10.

To identify the amino acids photolabeled in αV8–20, digestion with EndoLys-C was used, which generates fragments beginning at αHis−186 (containing αM1) and at αMet-242 (containing M2 and M3), which can be resolved by reversed-phase HPLC (Ziebell et al., 2004). When the EndoLys-C digests of αV8–20 were fractionated by reversed-phase HPLC (Fig. 5C), ~20% of ^{3}H was recovered in a hydrophobic peak centered at 90% organic, which by sequence analysis contained the fragment beginning at αMet-242 as the primary sequence and a single peak of ^{3}H release in cycle 20 corresponding to labeling of αGlu-262 (Open, 25 cpm/pmol; Des, 13 cpm/pmol) (Fig. 5D).

To identify the amino acids photolabeled in the δ subunit transmembrane domain, the photolabeled δ subunits were digested with EndoLys-C, which generates fragments of 10 to 14 kDa, one beginning at δPhe-206 and containing δM1 and another beginning at δMet-257 at the N terminus of δM2 and extending through δM3, that can be separated by reversed-phase HPLC after fractionation of the digests by Tricine-SDS PAGE (Arevalo et al., 2005). When the materials from these gel bands (Fig. 6A) were pooled and fractionated by reversed-phase HPLC (Fig. 6B), ~60% of ^{3}H was recovered in a peak at ~75% organic that contained the fragment beginning at δMet-257 as the primary sequence, and ~10% of ^{3}H was recovered in fractions eluting at ~ 60% organic that contained the fragment beginning at δPhe-206. For the fragment beginning at δMet-257, there was a major peak of ^{3}H release in cycle 20 (Fig. 6C), consistent with photolabeling of δM2–20 (δGln-276; Open, 1 cpm/pmol; Des, 0.3 cpm/pmol). For the fragment beginning at δPhe-206 (Fig. 6D), a single peak of ^{3}H release in cycle 31 indicated labeling within δM1 of δCys-236 (Open, 0.7 cpm/pmol; Des, 0.2 cpm/pmol).

Frozen-State Photolabeling of nAChRs Equilibrated with [^{3}H]Azietomidate. To compare with our previous results obtained with nAChRs in the desensitized state photolabeled in solution (Ziebell et al., 2004), we photolabeled nAChRs in the frozen state that had been equilibrated in

TABLE 2

State dependence of [^{3}H]azietomidate photoincorporation into residues in the nAChR transmembrane domain (cpm per picomole of PTH-derivative)

The level of ^{3}H incorporation in each residue was calculated from the observed ^{3}H release as described under *Materials and Methods*, and the mass was calculated from the initial and repetitive yield.

	50-ms [^{3}H]Azietomidate (Figs. 5 and 6)		Equilibrium [^{3}H]Azietomidate (Fig. 7)	
	Carb 50 ms	Carb Equilibrium	Carb 50 ms	Carb Equilibrium
Ion channel				
αM2–20 (αGlu-262)	25	13	67	42
δM2–20 (δGln-276)	1.0	0.5	1.7	1.0
δM2–24 (δGlu-280)	<0.04	<0.03	<0.1	<0.1
βM2–20 (βAsp-268)	N.D.	N.D.	4	N.D.
βM2–24 (βGlu-272)	N.D.	N.D.	<0.2	N.D.
δM1				
δCys-236	0.7	0.2	2	2
αMA/αM4				
αGlu-390	1.2	0.6	N.D.	N.D.
αHis-408	0.2	0.2		
αCys-412	0.8	0.4		

N.D., not determined.

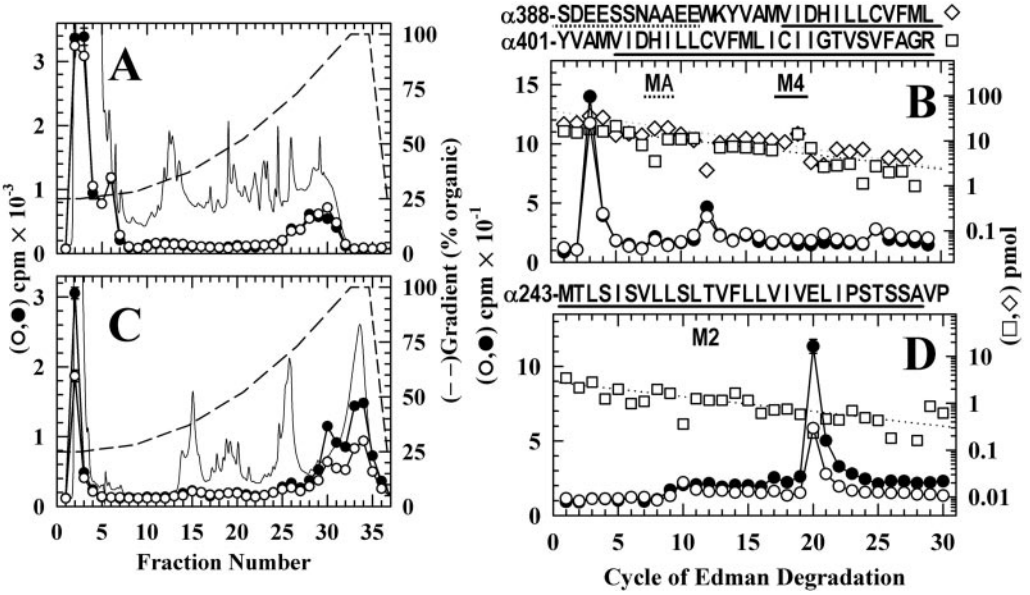

Fig. 5. Photolabeling in the nAChR α subunit transmembrane domain after 50-ms exposure to agonist and [^{3}H]azietomidate. nAChR-rich membranes (12 mg/condition) equilibrated without (Open, filled symbols) or with (Des, open symbols) 10 mM Carb were exposed to 10 μM [^{3}H]azietomidate + 10 mM Carb for 50 ms before freezing and photolabeling. After photolabeling, V8 protease digests of the α subunits were fractionated by SDS-PAGE and visualized by Coomassie blue stain, and material was eluted from the 10 kDa (αV8–10) and 20 kDa bands (αV8–20). The left panels are reversed-phase HPLC fractionations of (A) trypsin digests of αV8–10 samples (11,000 cpm injected each condition; recovery >90%) and (C) EndoLys-C digests of αV8–20 (●, 17,300 cpm injected; ○, 9600 cpm injected; 70% recoveries). Also included are the absorbance at 215 nm (dotted line) and the HPLC gradient (% organic). The right panels are ^{3}H (●, ○) and PTH-amino acids (◇, □) released during sequence analysis of nAChR subunit fragments beginning near the amino terminus of αM4 (pools of HPLC fractions 26–31 from A) (B), and αM2 (pools of HPLC fractions 29–31 from C) (D). The primary amino acid sequences are shown above each panel. B, each sample contained α subunit fragments beginning at αTyr-401 (Des, □, I_0 = 23 pmol; Open, I_0 = 16 pmol, not shown) and at αSer-388 (Des, ◇, I_0 = 46 pmol; Open, I_0 = 28 pmol, not shown). The major peak of ^{3}H release in cycle 3 indicated labeling of αGlu-390, and the minor peaks of ^{3}H release in cycles 12 and 25 indicated labeling of αCys-412 within the fragments beginning at αTyr-401 and αSer-388, respectively. D, each sample contained as the primary sequence the fragment beginning at αMet-243 at the N terminus of αM2 [Open and Des (□), I_0 = 2.9 pmol]. The peak of ^{3}H release in cycle 20 indicated labeling of αGlu-262. The pool of HPLC fractions 32 to 35 from C contained fragments beginning at αSer-173 (9 pmol, each condition) and at αMet-243 (7 pmol, each condition) and a single peak of ^{3}H release in cycle 20.

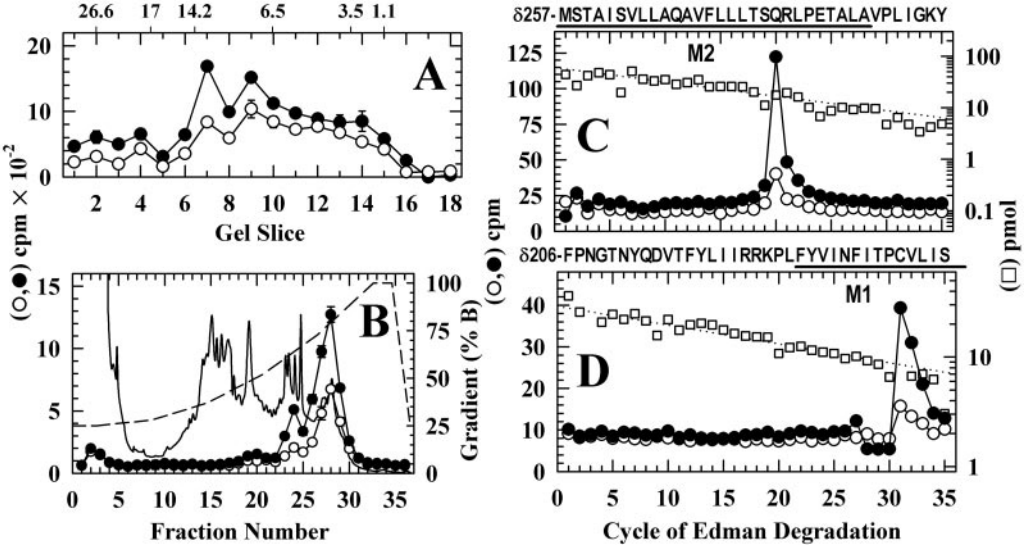

Fig. 6. Photolabeling in the nAChR δ subunit transmembrane domain after 50-ms exposure to agonist and [^{3}H]azietomidate. nAChR δ subunits isolated from the labeling described in Fig. 5 were digested with EndoLys-C and fractionated by Tricine SDS-PAGE. A, the distribution of ^{3}H eluted from 5-mm bands of the gel (Open, ●, 26,800 cpm loaded, 14,600 recovered; Des, ○, 17,400 cpm loaded, 10,200 cpm recovered). The mobilities of the molecular mass markers are indicated above the graph. B, reversed-phase HPLC fractionation of material eluted from gel bands 7–9 (●, 6350 cpm injected, 6000 recovered; ○, 4060 cpm injected, 3330 cpm recovered). Also included are the absorbance at 215 nm for the Des sample (solid line) and the HPLC gradient in percent organic phase (dashed line). The right panels are the ^{3}H (●, ○) and PTH-amino acids (□) released during sequence analysis of nAChR subunit fragments beginning at the amino terminus of δM2 (pools of HPLC fractions 26–29) (C) and M1 (pools of HPLC fractions 22–24) (D). C, the primary sequence began at δMet-257 at the N terminus of δM2 (Op, I_0 = 61 pmol, not shown; Des, □, I_0 = 60 pmol) and secondary sequences began at δAsn-437 (Open, 21 pmol; Des, 20 pmol) and δPhe-206 (Open, 3.7 pmol; Des, 2.8 pmol). The peak of ^{3}H release in cycle 20 was consistent with labeling at δGln-276 from the primary sequence detected. D, the primary sequence began at δPhe-206 before δM1 (Open, I_0 = 30 pmol, not shown; Des, □, I_0 = 29 pmol). The peak of ^{3}H release in cycle 31 indicated labeling of δCys-236.

solution with [^{3}H]azietomidate (18 μM) in the presence of a high concentration of 10 mM Carb, and then mixed with 10 mM Carb and frozen after 50-ms exposure. Membranes equilibrated with [^{3}H]azietomidate in the absence of agonist and then frozen after 50-ms exposure to Carb were also photolabeled in parallel.

To identify the amino acids photolabeled within αM2, the fragment beginning at αMet-242 at the N terminus of αM2 was isolated by reversed-phase HPLC from an EndoLys-C digest of αV8–20. Sequence analysis of that fragment (Fig. 7A) revealed a single major peak of ^{3}H release in cycle 20, corresponding to the labeling of αGlu-262. For nAChRs pre-equilibrated with [^{3}H]azietomidate and Carb (desensitized state), αGlu-262 was labeled at 40 cpm/pmol, whereas for the samples pre-equilibrated with [^{3}H]azietomidate alone and then exposed to Carb for 50 ms, αGlu-262 was labeled at 70 cpm/pmol.

To identify the amino acids photolabeled in δM2, the fragment beginning at δMet-257 at the N terminus of δM2 was purified by reversed-phase HPLC after fractionation of the δ subunit digest by Tricine-SDS PAGE. Sequence analysis of the fragment beginning at δMet-257 (Fig. 7B) revealed a single peak of ^{3}H release in cycle 20, consistent with labeling of δGln-276 at 1 cpm/pmol for the sample photolabeled in the desensitized state, and at 2 cpm/pmol for the sample prequilibrated with [^{3}H]azietomidate alone. Although for nAChRs photolabeled in solution δM2–2 and δM2–6 were labeled at 10 and 5% the level of δM2–20, for nAChRs photolabeled in the frozen state, the labeling of those positions, if it occurred, was at less than 5% the labeling of δM2–20.

We also characterized [^{3}H]azietomidate photolabeling within βM2, which had not been characterized previously. Digestion of the β subunit with trypsin generates a ~10-kDa fragment beginning at βMet-249, the N terminus of βM2, that can be isolated by Tricine-SDS-PAGE and HPLC purification (White and Cohen, 1992). For that fragment, which was sequenced only from nAChRs photolabeled after equilibration with [^{3}H]azietomidate in the absence of Carb, there was also only a single peak of ^{3}H release in cycle 20, consistent with labeling of βAsp-268 at 4 cpm/pmol (i.e., at a similar efficiency as δGln-276 and at ~5% the efficiency of αGlu-262).

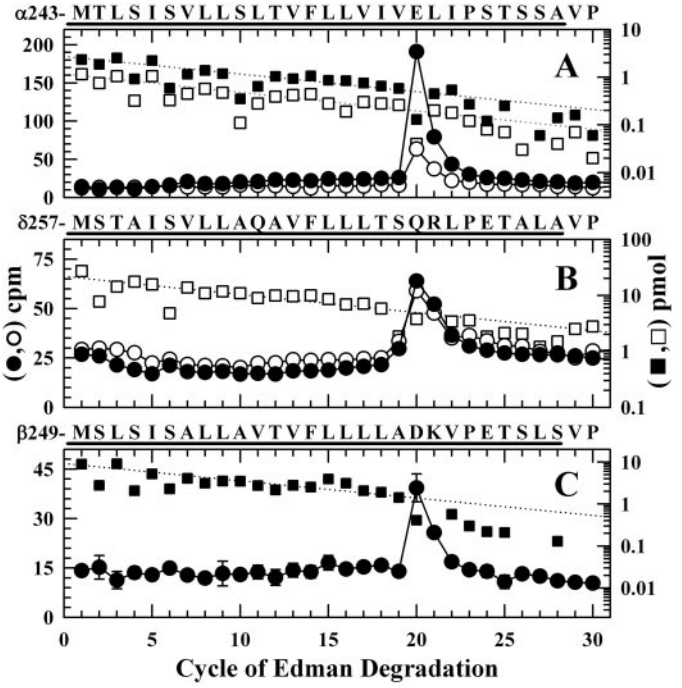

Fig. 7. Photolabeling after rapid-freezing of nAChRs equilibrated with [^{3}H]azietomidate and agonist. ^{3}H (●, ○) and PTH-amino acids (■, □) released during sequence analysis of nAChR subunit fragments beginning at the amino terminus of αM2 (A), δM2 (B), and βM2 (C). The primary amino acid sequences are shown above each panel. nAChR-rich membranes (12 mg/condition), pre-equilibrated with 18 μM [^{3}H]azietomidate either without (filled symbols) or with (open symbols) 10 mM Carb, were exposed to 10 mM Carb for 50 ms and then rapidly frozen for photolabeling. As described under *Materials and Methods*, the fragments containing αM2 were isolated by reversed-phase HPLC from EndoLys-C digests of αV8–20; the fragments containing at δM2 or βM2 were isolated from an EndoLys-C digests (δ subunit) or trypsin digests (β subunit) by Tricine-gel SDS-PAGE followed by reversed-phase HPLC. A, the primary sequence began at αMet-243 (■, I_0 = 2.7 pmol; □, I_0 = 1.2 pmol), and the peak of ^{3}H release in cycle 20 indicated labeling of αGlu-262. B, the primary sequence began at δMet-257 [□, I_0 = 22 pmol; not pre-equilibrated with Carb, I_0 = 19 pmol (not shown)]. The ^{3}H release in cycle 20 indicated labeling at δGln-276. C, the primary sequence began at the N terminus of βM2 (■, I_0 = 9.2 pmol) and a secondary sequence began at βLys-216 at the N terminus of βM1 (I_0 = 5.1 pmol, not shown). The ^{3}H release in cycle 20 indicated labeling at βAsp-268.

Discussion

We use rapid-perfusion electrophysiological techniques to establish that azietomidate acts primarily as an nAChR open-state inhibitor without enhancing the kinetics of desensitization. Full inhibition by 10 μM azietomidate develops within a second in the presence of ACh without any increase in the fraction of nAChRs in the desensitized state beyond that seen for ACh alone, and after removal of ACh, azietomidate did not stabilize nAChRs in the desensitized state. Because substantial inhibition develops after exposure to agonist and 10 μM azietomidate for 50 ms, these conditions were chosen for time-resolved photolabeling. Further studies, requiring a combination of single channel and rapid perfusion analyses, will be required to determine whether nAChR inhibition results from physical occlusion of the ion channel or from stabilization of the nAChR in a novel, nonconducting state.

The observed concentration-dependent increase in the rate of inhibition by azietomidate indicates that its apparent rate constant for open-state inhibition ($k_+ = 5 \times 10^5$ M^{-1} s^{-1}) is ~100-fold lower than that of the positively charged QX-222 (Dilger and Vidal, 1994) and ~10-fold lower than that of octanol and pentobarbital (Forman et al., 1995; Dilger et al., 1997). One factor that may account for azietomidate's low apparent rate constant is that it has a substantially higher lipid solubility (octanol/water partition coefficient, P = 3600) than octanol (P = 1400) or pentobarbital (P = 130). If the aqueous concentration determines the rate of inhibition, our calculation underestimates the value of k_+. Slow onset and recovery from inhibition are also reported for propofol (P = 4300; Dilger et al., 1994).

nAChR Photolabeling by [^{3}H]Azietomidate. In the nAChR structure (Fig. 8), the photolabeled amino acids are distributed in four different structural domains: 1) at the extracellular end of the ion channel (αM2–20, βM2–20, and δM2–20); 2) within the δ subunit helix bundle (δCys-236 in δM1); 3) in the cytoplasmic basket formed by the MA helices that precede the M4 helices in the primary structure (αGlu-390); and 4) at the lipid interface (αCys-412 in αM4). Also

included in Fig. 8 are Connolly surface representations (see *Materials and Methods*) of predicted azietomidate binding pockets within the ion channel near M2–20 (white), in the δ subunit helix bundle (blue), and in the nAChR cytoplasmic basket domain (yellow). Table 2 compares the efficiencies of [^{3}H]azietomidate incorporation in these structural domains. Although αGlu-262 is the residue photolabeled most efficiently, and it is plausible that binding to the extracellular end of the ion channel accounts for the functional inhibition of the nAChR, occupancy at the other sites could also contribute to inhibition. Additional photolabeling over a range of azietomidate concentrations would be required to determine the relative occupancy of each site.

The time-resolved photolabeling data in Table 2 show that the accessibility at the extracellular end of the ion channel and at the other sites are similar in the state(s) transiently stabilized by agonist and in the equilibrium desensitized state, because the same amino acids in each domain are photolabeled in both states at efficiencies that differ by less than 3-fold. However, [^{3}H]azietomidate cannot access the ion channel in the resting state (Ziebell et al., 2004). The other sites were not characterized in that study.

Photolabeling in the nAChR Ion Channel. Photolabeling of the nAChR with [^{3}H]azietomidate and other aliphatic diazirines has established that the activated intermediates react most efficiently with nucleophilic side chains (Glu, Asp, Tyr) (Pratt et al., 2000; Ziebell et al., 2004; Hamouda et al., 2006). Thus, the pattern of labeling of the glutamates and aspartates at the outer end of the channel (Table 2) likely delineates the binding pocket and orientation of azietomidate. That all of the M2–20, but none of the M2–24 (βGlu-272, δGlu-280) residues examined were photolabeled suggests that the pocket extends down the channel, which is lined by hydrophobic residues for ~15Å (Figs. 8, B and C). The homologous region in $GABA_A$Rs is lined with polar residues, providing a rationale for the much higher concentrations of azietomidate required to inhibit $GABA_A$Rs. Orientation may also explain why αGlu-262 is labeled >10-fold more efficiently than βM2–20 (βAsp-268), because there is no obvious structural or photochemical explanation. However, we cannot rule out the possibility that the unlabeled acidic side chains at position M2–24, which are oriented toward the channel in the resting state structure, have moved in the photolabeled conformations. Azioctanol also photolabels αM2–20 (αGlu-262) in the desensitized state (Pratt et al., 2000), and mutational analyses associate irreversible nAChR inhibition with reaction at αGlu-262 (Forman et al., 2007).

All of the above results are consistent with the preferred binding site for azietomidate being at the extracellular end of the ion channel. An alternative interpretation, based upon photolabeling studies of the nAChR in solution (Ziebell et al., 2004), was that the reactive amino acids at the extracellular end of the channel reacted with photoactivated azietomidate as it diffused into or out of an equilibrium binding site at the cytoplasmic end of the ion channel. This possibility was based upon the photolabeling of amino acids at the cytoplasmic end of the ion channel (Ser/Thr at positions M2–2 and M2–6 of the α and δ subunits) at ~1% the efficiency of αGlu-262 (Fig. 6C). In the frozen state photolabeling, however, the equilibrium binding is trapped and there would be no ongoing transient diffusion past M2–20.

Photolabeling in the δ Subunit Helix Bundle. The photolabeling in the presence of agonist of δM1 Cys-236, a residue that projects within the helix bundle, suggests that [^{3}H]azietomidate binds therein. In previous studies at 20°C, the fragment containing δM1 was photolabeled by [^{3}H]azietomidate in nAChRs in the desensitized, but not in the resting state (Ziebell et al., 2004). Within the nAChR structure (Fig. 8, C and D), which is believed to be the closed state, the pocket at the extracellular end of the δ subunit helix bundle, capped by the M2-M3 loop, is large enough to accommodate azietomidate, but it ends ~10 Å above the level of the

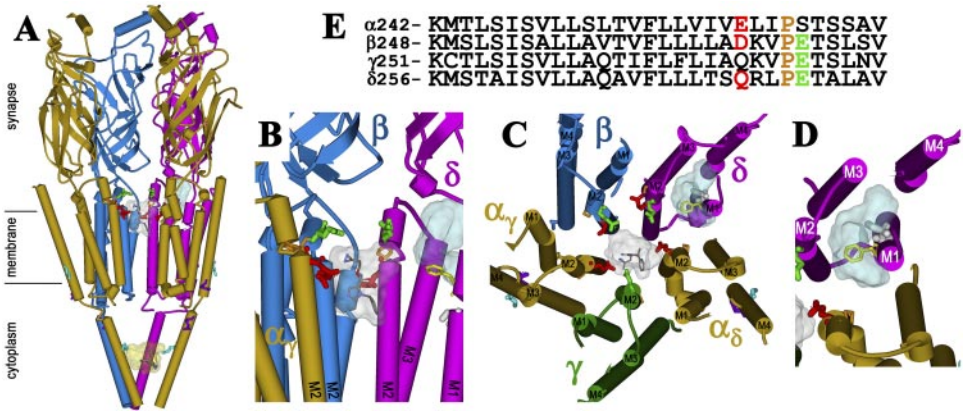

Fig. 8. The binding sites for [^{3}H]azietomidate in the nAChR. Views of the *T. marmorata* nAChR structure (Protein Data Bank code 2BG9) (α, gold; β, blue; γ, green; δ, magenta) showing α-helical (cylinders) and β-sheet (ribbon) secondary structure. A, a perspective parallel to the membrane surface (with the γ subunit omitted). B, an expanded view of A focused on the top of the channel (γ and α_δ omitted). C, the transmembrane helices viewed looking down the ion channel. D, the δ subunit helix bundle looking down the M1 helix. E, the amino acid sequences of each of the M2 helices of the nAChR structure, with the amino acids highlighted in the structures indicated by the same colors. The residues labeled by [^{3}H]azietomidate are shown in stick format, color-coded for location: ion channel, position M2–20 (αGlu-262, βAsp-269; and δ-Gln-276; red); the δ subunit helix bundle (δCys-236, white); αM4 (αCys-412; cyan); the cytoplasmic basket formed by the MA helices (αGlu-390, cyan). Also indicated in stick format in the M2 helices are unlabeled acidic side chains (βGlu-273 and δGlu-280; green) that project into the channel lumen and the prolines (orange) that precede those positions in each subunit. δPhe-232 (yellow), the amino acid in δM1 that is photolabeled by [^{125}I]TID (Arevalo et al., 2005) and [^{3}H]benzophenone (Garcia et al., 2007), is included, as are the amino acids in αMA/αM4 (αGlu-398, αAsp-407, purple) photolabeled by [^{3}H]azicholesterol (Hamouda et al., 2006). The volumes defined by the ensemble of the 10 lowest energy orientations of azietomidate docked at the extracellular end of the ion channel (gray, 680 Å^3), in the δ subunit helix bundle (blue, 570 Å^3), and in the cytoplasmic basket (yellow, 970 Å^3) are shown in Connolly surface representations with a single azietomidate docked in its lowest energy orientation in each pocket (see *Materials and Methods*).

labeled δCys-236, suggesting that activation causes the structure to change in this region.

Two other nAChR inhibitors photolabel within the δ subunit helix bundle in an agonist-dependent manner: [^{125}I]TID photolabels δCys-236, δPhe-232, δThr-274 (M2–18), δLeu-278 (M2–22), and δIle-288 (M2-M3 loop) at least 10 times more efficiently after transient exposure to agonist than in the equilibrium desensitized state (Arevalo et al., 2005; Hamouda et al., 2008), and [^{3}H]benzophenone photolabels δPhe-232, δPro-286, and δIle-288 at 20°C only in the presence of agonist (Garcia et al., 2007). However, the dramatic difference in [^{125}I]TID photolabeling between the transient and equilibrium agonist-stabilized states is in contrast to the <3-fold difference seen for [^{3}H]azietomidate photolabeling within the helix bundle. Although TID (vol. 150 Å^3) and benzophenone (vol. 125 Å^3) are both smaller than azietomidate (vol. 240 Å^3), 4-[3-(trifluoromethyl)-3*H*-diazirin-3-yl]-benzyl-1-(1-phenylethyl)-1*H*-imidazole-5-carboxylate (vol. 284 Å^3), a larger aryl diazirine, did not photolabel the δ subunit helix bundle in either resting or desensitized state (Nirthanan et al., 2008).

Photolabeling in the nAChR Cytoplasmic Domain. Azietomidate photolabeling of αGlu-390, within the basket formed by the MA helices that surround the cytoplasmic access to the ion channel (Fig. 8A), provides the first evidence that this region can act as a drug binding site. αGlu-390 is ~25 Å below the entry to the ion channel and oriented toward the interior of the basket near the base of the portals between each of the MA helices, where the basket dimensions are appropriate for an azietomidate binding site (Fig. 9). This is unlikely to be a random photolabeling event because azietomidate did not photolabel other negatively charged side chains in this region: αAsp-389, αGlu-391, αGlu-397, or αGlu-398. However, its affinity is likely to be lower than that of the channel because of the relative degree of photoincorporation in the two regions (Table 2). Further studies will be required to explore the site's functional significance, but we note that it is close to residues that control channel conductance in the α4β2 neuronal nAChR and the 5-HT$_{3A}$ receptor (Hales et al., 2006).

General Anesthetic Actions on Cys-Loop Receptors. Although azietomidate probably inhibits the nAChR via the ion channel site, our results provide direct evidence of the diversity of binding sites even for a single general anesthetic in a Cys-loop receptor. Anesthetic binding sites in GABA$_A$ and glycine receptors have been predicted to exist in the transmembrane domain within the pockets within the subunit helix bundles, where the volume of substituted side

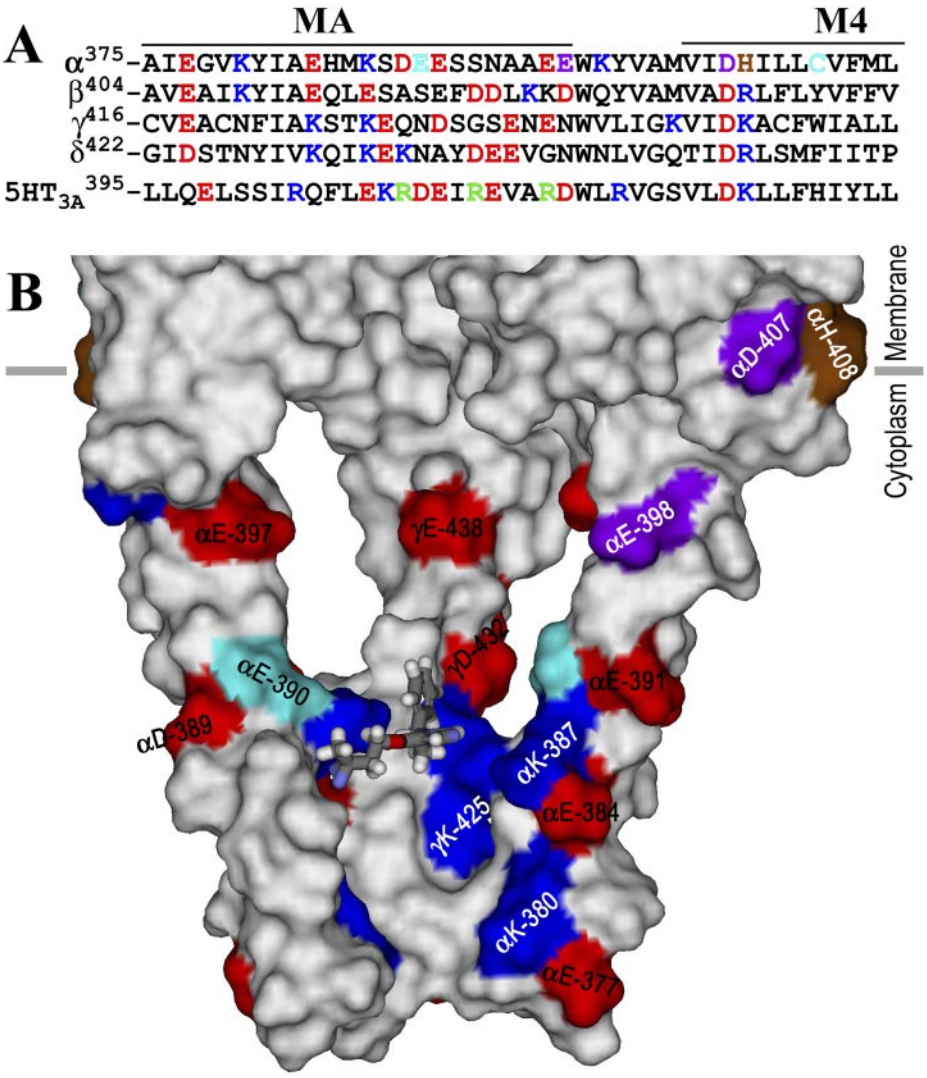

Fig. 9. An azietomidate binding pocket in the nAChR cytoplasmic domain. A, an alignment of the sequences of the *T. californica* nAChR subunit and human 5-HT$_{3A}$ receptor MA/M4 helices, with the positions in the nAChR α subunit photolabeled by [^{3}H]azietomidate, [^{3}H]azicholesterol (Hamouda et al., 2006), and [^{3}H]azioctanol (Pratt et al., 2000) colored cyan, purple, and brown, respectively. Other acidic and basic amino acids are colored red and blue, respectively. The positions in the 5-HT$_{3A}$ receptor identified as conductance determinants are green (Hales et al., 2006). B, a Connolly surface representation of the basket formed by the MA helices, viewed from the side with the β and δ subunits removed to visualize the interior and with the amino acids color-coded as in (A). An azietomidate molecule in stick format is included docked in its lowest energy orientation (see *Materials and Methods*).

chains determine the "cut-off" for the size of active anesthetics (Wick et al., 1998; Krasowski et al., 2001). [^{14}C]halothane (vol. 86 Å^3) binds within the nAChR δ subunit helix bundle in the absence or presence of agonist, whereas [^{3}H]azietomidate binds only in the presence of agonist, and the slightly larger [^{3}H]4-[3-(trifluoromethyl)-3*H*-diazirin-3-yl]benzyl-1-(1-phenylethyl)-1*H*-imidazole-5-carboxylate does not bind there but instead binds in the pocket at the interface between the α and γ subunits (Nirthanan et al., 2008). Our identification of an unexpected azietomidate binding site within the MA helix basket suggests that it will be important to determine whether this site is relevant for the action of anesthetics in other Cys-loop receptors.

References

Addona GH, Kloczewiak MA, and Miller KW (1999) Time-resolved photolabeling of membrane proteins: application to the nicotinic acetylcholine receptor. *Anal Biochem* **267:**135–140.

Arevalo E, Chiara DC, Forman SA, Cohen JB, and Miller KW (2005) Gating-enhanced accessibility of hydrophobic sites within the transmembrane region of the nicotinic acetylcholine receptor's delta-subunit - a time-resolved photolabeling study. *J Biol Chem* **280:**13631–13640.

Arias HR, Kem WR, Trudell JR, and Blanton MP (2003) Unique general anesthetic binding sites within distinct conformational states of the nicotinic acetylcholine receptor. *Int Rev Neurobiol* **54:**1–50.

Borghese CM, Ali DN, Bleck V, and Harris RA (2002) Acetylcholine and alcohol sensitivity of neuronal nicotinic acetylcholine receptors: mutations in transmembrane domains. *Alcohol Clin Exp Res* **26:**1764–1772.

Chiara DC, Trinidad JC, Wang D, Ziebell MR, Sullivan D, and Cohen JB (2003) Identification of amino acids in the nicotinic acetylcholine receptor agonist binding site and ion channel photolabeled by 4-[(3-trifluoromethyl)-3*H*-diazirin-3-yl]benzoyllcholine, a novel photoaffinity antagonist. *Biochemistry* **42:**271–283.

Dilger JP and Vidal AM (1994) Cooperative interactions between general anesthetics and QX-222 within the pore of the acetylcholine receptor ion channel. *Mol Pharmacol* **46:**169–175.

Dilger JP, Vidal AM, Mody HI, and Liu Y (1994) Evidence for direct actions of general anesthetics on an ion channel protein. *Anesthesiology* **81:**431–442.

Dilger JP, Boguslavsky R, Barann M, Katz T, and Vidal AM (1997) Mechansims of barbiturate inhibition of acetylcholine receptor channels. *J Gen Physiol* **109:**401–414.

Forman SA (1999) A hydrophobic photolabel inhibits nicotinic acetylcholine receptors via open-channel block following a slow step. *Biochemistry* **38:**14559–14564.

Forman SA, Firestone LL, and Miller KW (1987) Is agonist self-inhibition at the nicotinic acetylcholine receptor a nonspecific action? *Biochemistry* **26:**2807–2814.

Forman SA, Miller KW, and Yellen G (1995) A discrete site for general anesthetics on a postsynaptic receptor. *Mol Pharmacol* **48:**574–581.

Forman SA, Zhou QL, and Stewart DS (2007) Photoactivated 3-azioctanol irreversibly desensitizes muscle nicotinic ACh receptors *via* interactions at αE262. *Biochemistry* **46:**11911–11918.

Garcia G 3rd, Chiara DC, Nirthanan S, Hamouda AK, Stewart DS, and Cohen JB (2007) [^{3}H]Benzophenone photolabeling identifies state-dependent changes in nicotinic acetylcholine receptor structure. *Biochemistry* **46:**10296–10307.

Hales TG, Dunlop JI, Deeb TZ, Carland JE, Kelley SP, Lambert JJ, and Peters JA (2006) Common determinants of single channel conductance within the large cytoplasmic loop of 5-hydroxytryptamine type 3 and alpha(4)beta(2) nicotinic acetylcholinerReceptors. *J Biol Chem* **281:**8062–8071.

Hamouda AK, Chiara DC, Blanton MP, and Cohen JB (2008) Probing the structure of the affinity-purified and lipid-reconstituted *Torpedo* nicotinic acetylcholine receptor. *Biochemistry* **47:**12787–12794.

Hamouda AK, Chiara DC, Sauls D, Cohen JB, and Blanton MP (2006) Cholesterol interacts with transmembrane alpha-helices M1, M3, and M4 of the *Torpedo* nicotinic acetylcholine receptor: photolabeling studies using [^{3}H]azicholesterol. *Biochemistry* **45:**976–986.

Hemmings HC Jr, Akabas MH, Goldstein PA, Trudell JR, Orser BA, and Harrison NL (2005) Emerging molecular mechanisms of general anesthetic action. *Trends Pharmacol Sci* **26:**503–510.

Hess GP, Cash DJ, and Aoshima H (1983) Acetylcholine receptor-controlled ion translocation: Chemical kinetic investigations of the mechanism. *Annu Rev Biophys Bioeng* **12:**443–473.

Husain SS, Ziebell MR, Ruesch D, Hong F, Arevalo E, Kosterlitz JA, Olsen RW, Forman SA, Cohen JB, and Miller KW (2003) 2-(3-Methyl-3*H*-diaziren-3-yl)ethyl 1-(1-phenylethyl)-1*H*-imidazole-5- carboxylate: a derivative of the stereoselective general anesthetic etomidate for photolabeling ligand-gated ion channels. *J Med Chem* **46:**1257–1265.

Kotzyba-Hibert F, Kapfer I, and Goeldner M (1995) Recent trends in photoaffinity labeling. *Angew Chem Int Ed* **34:**1296–1312.

Krasowski MD, Nishikawa K, Nikolaeva N, Lin A, and Harrison NL (2001) Methionine 286 in transmembrane domain 3 of the $GABA_A$ receptor β subunit controls a binding cavity for propofol and other alkylphenol general anesthetics. *Neuropharmacology* **41:**952–964.

Lape R, Colquhoun D, and Sivilotti LG (2008) On the nature of partial agonism in the nicotinic receptor superfamily. *Nature* **454:**722–727.

Li GD, Chiara DC, Sawyer GW, Husain SS, Olsen RW, and Cohen JB (2006) Identification of a $GABA_A$ receptor anesthetic binding site at subunit interfaces by photolabeling with an etomidate analog. *J Neurosci* **26:**11599–11605.

Liao M, Sonner JM, Husain SS, Miller KW, Jurd R, Rudolph U, and Eger EI 2nd (2005) (+) Etomidate and the photoactivable R (+) azietomidate have comparable anesthetic activity in wild-type mice and comparably decreased activity in mice with a N265M point mutation in the gamma-aminobutyric acid receptor β3 subunit. *Anesth Analg* **101:**131–135.

Maconochie DJ and Steinbach JH (1998) The channel opening rate of adult- and fetal-type mouse muscle nicotinic receptors activated by acetylcholine. *J Physiol-London* **506:**53–72.

Middleton RE and Cohen JB (1991) Mapping of the acetylcholine binding site of the nicotinic acetylcholine receptor: [^{3}H]nicotine as an agonist photoaffinity label. *Biochemistry* **30:**6987–6997.

Mourot A, Grutter T, Goeldner M, and Kotzyba-Hibert F (2006) Dynamic structural investigations on the *Torpedo* nicotinic acetylcholine receptor by time-resolved Photoaffinity labeling. *Chembiochem* **7:**570–583.

Nirthanan S, Garcia G 3rd, Chiara DC, Husain SS, and Cohen JB (2008) Identification of binding sites in the nicotinic acetylcholine receptor for TDBzl-etomidate, a photoreactive positive allosteric effector. *J Biol Chem* **283:**22051–22062.

Pratt MB, Husain SS, Miller KW, and Cohen JB (2000) Identification of sites of incorporation in the nicotinic acetylcholine receptor of a photoactivatible general anesthetic. *J Biol Chem* **275:**29441–29451.

Schägger H and von Jagow G (1987) Tricine-sodium dodecyl sulfate-polyacrylamide gel electrophoresis for the separation of proteins in the range From 1 to 100 kDa. *Anal Biochem* **166:**368–379.

Sullivan DA and Cohen JB (2000) Mapping the agonist binding site of the nicotinic acetylcholine receptor: orientation requirements for activation by covalent agonist. *J Biol Chem* **275:**12651–12660.

Unwin N (2005) Refined structure of the nicotinic acetylcholine receptor at 4 Å resolution. *J Mol Biol* **346:**967–989.

Vodovozova EL (2007) Photoaffinity labeling and its application in structural biology. *Biochemistry-Moscow* **72:**1–20.

Wenningmann I, Barann M, Vidal AM, and Dilger JP (2001) The effects of isoflurane on acetylcholine receptor channels: 3. effects of conservative polar-to-nonpolar mutations within the channel pore. *Mol Pharmacol* **60:**584–594.

White BH and Cohen JB (1988) Photolabeling of membrane-bound *Torpedo* nicotinic acetylcholine receptor with the hydrophobic probe 3-trifluoromethyl-3-(*m*-[^{125}I]iodophenyl)diazirine. *Biochemistry* **27:**8741–8751.

White BH and Cohen JB (1992) Agonist-induced changes in the structure of the acetylcholine receptor M2 regions revealed by photoincorporation of an uncharged nicotinic non-competitive antagonist. *J Biol Chem* **267:**15770–15783.

Wick MJ, Mihic SJ, Ueno S, Mascia MP, Trudell JR, Brozowski SJ, Ye Q, Harrison NL, and Harris RA (1998) Mutations of gamma-aminobutyric acid and glycine receptors change alcohol cutoff: evidence for an alcohol receptor? *Proc Natl Acad Sci U S A* **95:**6504–6509.

Yamakura T, Bertaccini E, Trudell JR, and Harris RA (2001) Anesthetics and ion channels: molecular models and sites of action. *Annu Rev Pharmacol Toxicol* **41:**23–51.

Zhou QL, Zhou Q, and Forman SA (2000) The n-alcohol site in the nicotinic receptor pore is a hydrophobic patch. *Biochemistry* **39:**14920–14926.

Ziebell MR, Nirthanan S, Husain SS, Miller KW, and Cohen JB (2004) Identification of binding sites in the nicotinic acetylcholine receptor for [^{3}H]azietomidate, a photoactivatable general anesthetic. *J Biol Chem* **279:**17640–17649.

Address correspondence to: Jonathan B. Cohen, Dept. of Neurobiology, Harvard Medical School, 220 Longwood Ave., Boston, MA 02115. E-mail: jonathan_cohen@hms.harvard.edu